Near-threshold study of Xe 3*d* photoionization

A. Kivimäki,[1] U. Hergenhahn,[2,3] B. Kempgens,[2] R. Hentges,[2] M. N. Piancastelli,[2,4] K. Maier,[2] A. Rüdel,[2] J. J. Tulkki,[5] and A. M. Bradshaw[3]

[1]*Department of Physical Sciences, P.O. Box 3000, 90014 University of Oulu, Finland*
[2]*Fritz-Haber-Institut der Max-Planck-Gesellschaft, Faradayweg 4-6, 14195 Berlin, Germany*
[3]*Max-Planck-Institut für Plasmaphysik, Boltzmannstrasse 2, 85748 Garching, Germany*
[4]*Department of Chemical Sciences and Technologies, University ''Tor Vergata,'' 00133 Rome, Italy*
[5]*Helsinki University of Technology, Laboratory of Computational Engineering, P.O. Box 9400, 02015 HUT, Finland*

(Received 14 June 2000; published 13 December 2000)

The 3*d* photoelectron spectrum of xenon has been measured at several photon energies in the immediate threshold region. The absolute photoionization cross section and angular anisotropy parameter β have been determined for the two spin-orbit-split components. The experimental results are compared with calculations using a relaxed single-channel approximation. In agreement with theory, most abrupt changes in cross section and angular distribution are observed just above threshold. However, the Xe $3d_{5/2}$ photoionization cross section also reveals, some 30-eV above threshold a second maximum that has not been predicted theoretically.

DOI: 10.1103/PhysRevA.63.012716 PACS number(s): 32.80.Hd, 32.80.Fb

I. INTRODUCTION

Photoionization from the inner shell 3*d* of Xe has been studied much less extensively than that from the more shallow 4*d* level or from the outer shells 5*p* and 5*s*. Siegbahn *et al.* measured the Xe 3*d* photoelectron spectrum, and determined the binding energies of the corresponding core-ionized states [1]. A wider 3*d* photoelectron spectrum, including shake-up satellites, was published later [2]. From the total widths of the photoelectron lines measured using Al $K\alpha$ radiation, the lifetime broadening of the $3d^{-1}$ states was estimated to be ~0.5 eV [3]. The absorption spectrum of xenon at the 3*d* threshold was reported in absolute units by Deslattes [4] and Yağci and Wilson [5]. Arp *et al.* [6] recently published a total-ion-yield spectrum of the 3*d* threshold region.

The Xe 3*d* absorption spectrum shows two broad and intense maxima (Fig. 1) that are centered some 11 eV above the spin-orbit-split 3*d* ionization thresholds ($3d_{5/2}$: 676.4 eV [1]). They have been attributed to the $3d \rightarrow \epsilon f$ shape resonances. Superimposed on these, one can see some weaker features, the nature of which is not entirely clear. The resonances preceding the $3d_{3/2}$ edge have been interpreted as due to the $3d_{3/2} \rightarrow 6p, 7p$ excitations [5,6]. However, in recent investigations of the $M_{4,5}$-$N_{4,5}N_{4,5}$ normal Auger electron spectra [7] there was no evidence of additional lines due to spectator decay of the $3d_{3/2}^{-1}np$ vacancy state.

This problem can be solved in principle by studying the partial 3*d* photoionization cross sections. The only experimental investigation so far in this direction was performed by Becker *et al.* [8], who also determined the angular distribution of the 3*d* photoelectrons. The photon energy range studied extended from just above threshold to 1000 eV. Unfortunately, the photon energy resolution was not sufficient to detect whether or not resonances around 690 eV affect the 3*d* single-hole photoionization cross section. At higher photon energies the results agreed reasonably well with the results of Hartree-Fock calculations [9]. But, in disagreement with both the calculation and the absorption spectrum, the partial cross sections of Ref. [8] increased toward threshold even at the lowest photon energies. In the present paper we study Xe 3*d* photoionization with high resolution, particularly in the threshold region, in order to resolve these discrepancies. We report results for the partial photoionization cross sections of both spin-orbit split components in absolute units (Sec. IV A). The angular distribution parameter β is also measured in a backscattering geometry and, for the $3d_{5/2}$ line, in the dipole plane perpendicular to the light beam (Sec. IV C).

II. EXPERIMENT

A. Experimental setups

Most measurements were carried out on the soft-x-ray undulator beamline X1B [10] at the National Synchrotron

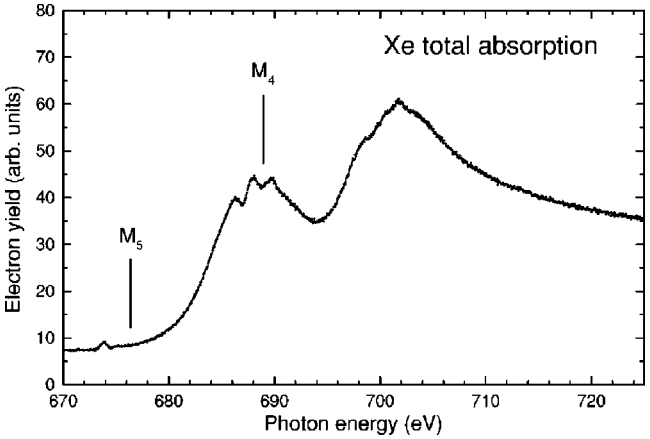

FIG. 1. The absorption spectrum of Xe at the 3*d* threshold region measured as a yield of secondary electrons ($E_{\mathrm{kin}} \sim 0.5$ eV). Entrance and exit slits of 30 and 40 μm were used for the monochromator, and a 300-eV pass energy for the electron analyzer. The photon energy scale follows Ref. [6] for the positions of the spectral features. The vertical bars marked with M_5 and M_4 indicate the 3*d* ionization thresholds, as given in Ref. [1].

Light Source, Brookhaven. The spherical grating monochromator employs the Dragon geometry [11] and is equipped with a holographically manufactured laminar grating (800 lines/mm). The monochromatized radiation is sufficiently intense for gas-phase photoelectron spectroscopy from 250 to 1000 eV, while still offering reasonably high-photon-energy resolution: The use of the 30 (40) μm openings for the entrance (exit) slits of the monochromator resulted in photon bandwidths narrower than 500 meV at a photon energy of ~700 eV and—employing the analyser described below—count rates of 2 kHz on the Xe $3d$ line.

Monochromatized radiation enters the interaction region along the main symmetry axis of the spatially fixed cylindrical mirror analyzer (CMA) [12]. Electrons ejected backward into the magical angle of 54.7° with respect to the axis can enter the analyzer. A circular microchannel plate detector (with a central hole) is placed on the CMA axis in front of the focal point of the analyzer such that electrons of a given kinetic energy form a circular distribution pattern. The plane of the detector thus includes electric and magnetic vectors of the incident light. The detector is divided into eight segments, each of which spans 45° azimuthally. A spherical entrance lens can be used to retard the electrons before they enter the cylindrical capacitor. In this study, the CMA was operated with a fixed 40-eV pass energy (E_{pass}), which corresponds to a ~250-meV kinetic-energy resolution.

Additional measurements were done with a different setup. A rotatable UHV chamber equipped with three time-of-flight analyzers similar to the type described by Hemmers *et al.* [13] was used on the BW3 beamline at the Hamburger Synchrotronstrahlungslabor HASYLAB at DESY, Hamburg. The analysers were mounted in the dipole plane. Spectra were taken at two different positions of the chamber angle, with analyzers positioned at −54.7°, 90°, and 180° rotation angles relative to the electric-field vector, and with the first analyzer positioned at −15°.

B. Geometrical considerations

Within the dipole approximation, the differential cross section of an electron line under a 54.7° backscattering geometry is [14]

$$\frac{d\sigma}{d\Omega}=\frac{\sigma}{4\pi}\left[1+\frac{1}{2}\beta P\cos 2\phi\right], \tag{1}$$

where σ is the total cross section, β is the angular anisotropy parameter, and $P=(I_x-I_y)/(I_x+I_y)$ is the degree of linear polarization (the first Stokes parameter). I_x and I_y denote radiation intensities measured with plane polarizers parallel and perpendicular to the storage ring plane, respectively. ϕ is the angle between the electric vector and the projection of the direction of observation on the detector plane. As long as the dipole approximation is valid, the β values of electron lines can be determined directly from the intensities observed in different segments; the summed intensity of the eight segments is proportional to the cross section.

The geometry used in the present measurements leads, within the dipole approximation, to a simple equation for the angular asymmetry parameter β of a given electron line [12]:

$$\beta P=\frac{\pi}{\sqrt{2}}\frac{I_1-I_3+I_5-I_7}{I_1+I_3+I_5+I_7}. \tag{2}$$

Here I_i is the integrated electron intensity in the detector segment i. Segments 1 and 5 are horizontal, and are bisected by the plane containing the electric and propagation vectors of the incident light. Segments 3 and 7 are located symmetrically about the perpendicular plane that contains the light propagation vector.

In recent years, it was theoretically predicted [15,16] and experimentally verified [17] that nondipole effects can already be significant at photon energies well below 1000 eV (also see Ref. [18] for a recent review). When we take into account the first-order ($E2$ and $M1$) corrections to the differential cross section of photoelectron lines [15], and transform to a right-handed coordinate system with the z axis pointing in the direction of photon propagation and the x axis lying in the storage ring plane, we obtain

$$\frac{d\sigma}{d\Omega}=\frac{\sigma}{4\pi}\left[1-\frac{\beta}{2}\left(P_2(\cos\theta)-\frac{3}{2}P\cos 2\phi\sin^2\theta\right)+\delta\cos\theta+\frac{1}{2}\gamma(1+P\cos 2\phi)\cos\theta\sin^2\theta\right]. \tag{3}$$

Here δ and γ describe ($E1$-$M1$) and ($E1$-$E2$) interference terms, and are defined as in Ref. [16]. θ is measured from the z axis to the electron propagation direction. It is assumed that the main axis of the light polarization ellipse aligns with x. From this equation, it is seen that inclusion of the higher multipoles leads to a redistribution of intensity between forward and backward scattering angles, which is described by the $\delta\cos\theta$ and $(\gamma/2)\cos\theta$ terms. Inserting our spectrometer angle $\theta=125.3°$, Eq. (1) should be modified to the form

$$\frac{d\sigma}{d\Omega}=\frac{\sigma}{4\pi}\left[1-\frac{\delta}{\sqrt{3}}-\frac{\gamma}{3\sqrt{3}}+\left(\frac{\beta}{2}-\frac{\gamma}{3\sqrt{3}}\right)P\cos 2\phi\right]. \tag{4}$$

Angle-integrated as well as angle-resolved results are therefore modified as a consequence of the higher-order terms. The quantity extracted by an analysis of the measured asymmetry according to Eq. (2) can be written as a modified angular distribution parameter β', connected to the dipole β by

$$\beta'=\beta-\frac{2\gamma}{3\sqrt{3}}. \tag{5}$$

For the present case of Xe $3d$ photoemission, however, values below ± 0.02 for δ and γ are to be expected from a theoretical study [16]. We will therefore proceed with the analysis of partial cross sections and angular anisotropies according to Eq. (1), and discuss possible modifications due to higher-order terms at a later point in the text.

C. Data reduction

The Xe $3d$ photoelectron spectra were normalized to the pressure of the target gas and the photon flux. In addition, to account for possible changes in the response of the photodi-

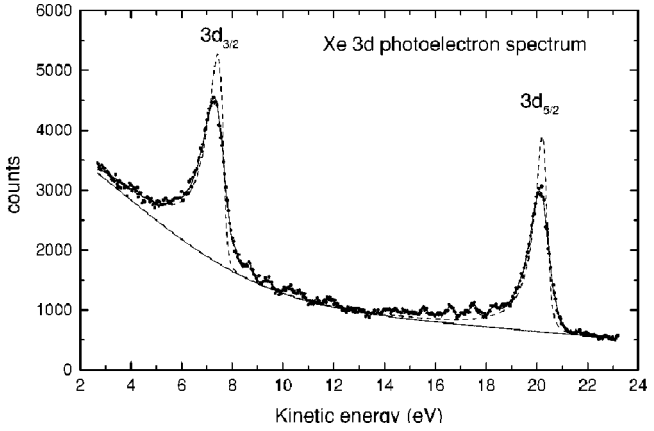

FIG. 2. The 3d photoelectron spectrum of Xe measured at 697-eV photon energy. Experimental data are shown with dots. The broken curves depict the inherent line shapes of the photoelectron lines, made asymmetric by PCI. The inherent line shapes of Auger transitions (weaker structures) were described by Lorentzians (not shown). The full line gives the final fit result after convolution with the instrumental profiles.

ode to the flux during the measurement (e.g., due to the changes in the beam position), the Ne 2p photoelectron spectrum was recorded before and after each Xe 3d measurement. The normalized intensity $I_{3d_i}(h\nu)$ of the $3d_i$ photoelectron line ($i=3/2,5/2$) at a photon energy $h\nu$ is obtained from the fit (see below). The corresponding unscaled partial photoionization cross section $\sigma_i(h\nu)$ can then be calculated from

$$\sigma_{3d_i}(h\nu)=I_{3d_i}(h\nu)*\sigma_{\mathrm{Ne}\ 2p}(h\nu)/I_{\mathrm{Ne}\ 2p}(h\nu), \qquad (6)$$

where $\sigma_{\mathrm{Ne}\,2p}$ and $I_{\mathrm{Ne}\,2p}$ are the cross section [19] and normalized average intensity of the Ne 2p photoelectron line, respectively, at the same photon energy. Note that for the determination of the cross section, the accuracy of the absolute $\sigma_{\mathrm{Ne}\,2p}$ values is not critical; more important is that its attenuation as a function of photon energy is correctly described. This fact limits the systematical inaccuracy of the method resulting from the neglect of the influence of δ and γ on $\sigma_{\mathrm{Ne}\,2p}$, which was measured in Ref. [17], to below 1.5%.

The Ne 2s photoelectron line, the β parameter of which is 2, was measured in order to determine the degree of linear polarization P. However, in the present geometry the nonzero γ parameter affects the observed angular distribution ($\delta=0$ for s photoelectron lines). Using the results of Hemmers and co-workers [17,20] for γ, P was found to be 0.74, and is thus higher than the apparent value of 0.70 given by Eq. (2). For the measurements performed on the BW3 beamline at HASYLAB, the degree of linear polarization P is of less concern: a value of 0.97 or larger is routinely determined for P from the results of angle-resolved photoelectron spectroscopy.

Figure 2 shows the electron spectrum of xenon taken at 697-eV photon energy. The original data have been corrected for the transmission function of the analyzer. The two most intense peaks are the $3d_{3/2}$ and $3d_{5/2}$ photoelectron lines. They show characteristic tails towards lower kinetic energies due to post-collision interaction (PCI) between the photoelectron and the subsequently emitted Auger electron. The Auger electron is much faster than the photoelectron (e.g., the decay process $3d^{-1}\rightarrow 4d^{-2}$ leads to Auger kinetic energies of about 520 eV); hence it can overtake the latter, which results in an energy exchange between the two electrons.

As an approximation to the line shape the analytical profile derived by Armen *et al.* [21] for coincident experiments has been implemented in our nonlinear least-squares fit program. The broken curves in Fig. 2 depict this intrinsic line shape before convolution with the instrumental profiles. The spectrum of Fig. 2 also contains considerable intensity due to Auger transitions. Not only the $N_{4,5}$-OO diagram Auger lines and their correlation satellites [22] but also cascade processes following the first-step Auger decay (e.g., $3d^{-1}\rightarrow 4d^{-2}\rightarrow 4d^{-1}5p^{-2}\rightarrow 5p^{-4}$) are expected to contribute to the features seen in the spectrum of Fig. 2. Indeed, the height of the background at low kinetic energies was observed to correlate with the changes of the 3d photoionization cross section.

The presence of Auger lines makes it more difficult to derive the intensities of the photoelectron lines. The kinetic energies of the Auger lines that appeared to arise from 4d photoionization were taken from Ref. [22]. These Auger lines were also used for the kinetic-energy calibration. When there was overlap between 3d photoelectron lines and Auger lines at certain photon energies, the intensities of the Auger lines were approximated from measurements done at nearby photon energies and kept fixed.

In principle, the fit program can be used to extract the lifetime widths of the $3d^{-1}$ states. The Lorentzian lifetime broadenings of the 3d photoelectron lines were therefore allowed to vary within certain limits in the first fits. However, when the results did not converge at a single value; the lifetime widths were fixed to 0.5 eV [3]. The failure to obtain the lifetime broadening may at least partly be attributed to ''interfering'' Auger lines. In the fit, a Gaussian function represented the monochromator bandwidth; its width was calculated analytically for each photon energy. A predetermined numerical profile was used for the shape of the spectrometer broadening, with a width set according to the investigated behavior of the electron energy resolution as a function of E_{kin}/E_{pass} [23].

III. CALCULATIONS

No theoretical data for the Xe 3d photoionization separated into the spin-orbit-split components are known to us. We have therefore calculated the partial cross sections and the β parameter using a fully relativistic *ab initio* code [24], based on the atomic structure program of Grant et al. [25]. The continuum wave function of the outgoing photoelectron was calculated using separately optimized final-state orbitals for the photoion. This takes into account the ''intrachannel'' correlations, which is another way of saying that the total final state wavefunctions diagonalize the total final-state Hamiltonian, $\langle\psi_E|H|\psi_{E'}\rangle=E\,\delta(E-E')$, where ψ refers to the same ionic state. Exchange effects in the continuum and

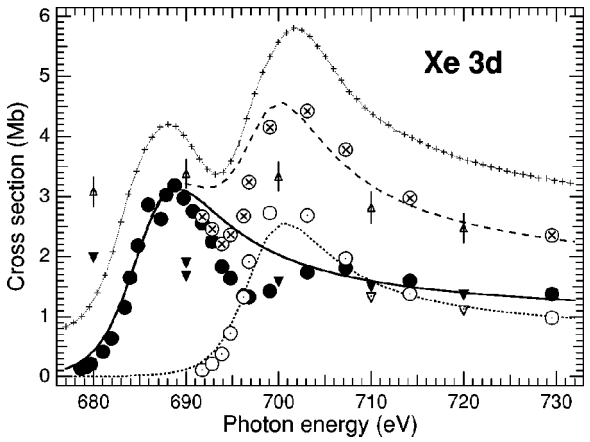

FIG. 3. The $3d_{3/2,5/2}$ photoionization cross sections. Closed and open circles give the experimental cross sections of the $3d_{5/2}$ and $3d_{3/2}$ photoelectron lines, respectively, determined from the measurements that were performed at the X1B beamline. Crossed circles denote their sum, i.e., total $3d$ single-hole photoionization cross section. Also shown are the corresponding results from Becker *et al.* [8] (closed and open triangles and up-triangles with error bars). The solid, dotted, and dashed curves give the calculated $3d_{5/2}$, $3d_{3/2}$, and $3d$ photoionization cross sections, shifted in energy by -5.1 eV. The uppermost curve is the measured total photoabsorption cross section of Xe [29].

overlap matrix elements appropriate to quantify relaxation effects were included. This scheme was termed the atomic-state-function approximation in Ref. [24], and proved successful for the explanation of the Kr $3d$ partial photoionization cross section.

IV. RESULTS

A. Cross section

The scaling of the normalized intensities of the photoelectron lines [Eq. (6)] to the absolute cross section can usually be done with the aid of a photoabsorption spectrum measured in absolute units. First the contribution of the partial photoionization cross sections of less deeply bound shells should be estimated. This can be done by extrapolating the shape of the photoabsorption cross section from below to above the edge of interest by the Victoreen formula [26]. At the Xe $3d$ threshold there is, however, interchannel coupling between different photoionization processes [27,28], i.e., the partial photoionization cross sections of other shells, particularly of $4d$, are affected by the emergence of the $3d$ channels. We have therefore used the data of Becker and coworkers [8,27] to scale our $3d$ partial photoionization cross section to their value (2.35 Mb) at 730-eV photon energy. There are no abrupt changes in photoabsorption at this photon energy, so the scaling is not sensitive to the photon energy resolution. The resulting $3d$ partial photoionization cross sections are shown in Fig. 3. Also included is the photoabsorption spectrum taken from Ref. [29]. Note that it was determined in absolute units independently of a calibrant gas using the setup described in Ref. [30].

The difference between the photoabsorption and the sum of the partial $3d$ photoionization cross sections at 730 eV is about 0.9 Mb. Becker et al. [27] also determined photoionization cross sections for the shallower main lines and their satellites. These add up to about 0.63 Mb at $h\nu = 730$ eV, which leaves 0.2–0.3 Mb for such shake-up and shake-off transitions that accompany $3d$ ionization. It would be quite difficult to verify the contribution of the $3d$ shake-up processes at low kinetic energies, since they have intensities comparable to overlapping $4d$-based Auger lines. From a measurement performed at 835-eV photon energy, however, we extracted the total intensity of shake-up lines to be $\sim$10% of that of the $3d$ main lines. The above figures can also be compared to the photoabsorption cross section just before the $3d$ threshold, which is $\sim$0.66 Mb, and originates from all possible photoionization processes from shallower shells, including shake-up and shake-off transitions. The contribution of these processes is thus very similar to the result ($\sim$0.63 Mb) of Becker *et al.*[27] at $h\nu = 730$ eV, which indicates that the scaling should not be too much in error.

Becker and co-workers [8,27] gave an uncertainty of about ± 0.25 Mb for their determination of the photoionization cross sections at $h\nu = 730$ eV. When using their results for scaling, the same uncertainty is directly transferred to our results, making it the largest absolute source of error. As noted above, the neglect of nondipole effects in Ne $2p$ photoionization causes a systematic normalization error ($<$1.5%). Another factor that can be categorized under normalization errors arises from fluctuations of incident photon flux; this is estimated to be below 3%. Statistical errors cause an uncertainty of similar magnitude in most measurements, but it could be considerably larger in the measurements done just a few eV above threshold, where the cross section is low and the shape of the background most difficult to estimate. An important source of error at very low kinetic energies arises from the uncertainty of the transmission function of the electron analyzer. The errors due to variations in the target gas pressure, on the contrary, are negligible, since pressure was continuously monitored. We estimate the total error excluding scaling to be less than 10% for measurements performed more than 10 eV above each threshold.

The $3d$ photoionization cross section gradually increases on going from threshold toward higher excitation energies, as might be expected from the behavior of the total photoabsorption cross section. The first small resonance (at 686 eV) on the $3d_{5/2} \rightarrow \epsilon f$ shape resonance might cause a variation to the $3d_{5/2}$ photoionization cross section. Any effect on the other two resonances cannot be seen in this curve, but the paucity of data points and the magnitude of error bars could conceal it. However, it is clear that there is another broad maximum in the $3d_{5/2}$ photoionization cross section around 707 eV (or some 30 eV above threshold). Starting from threshold, the cross section curve for $3d_{3/2}$ is very similar to that for $3d_{5/2}$, when the curves are inspected as a function of photoelectron kinetic energy. They even appear to achieve the same absolute cross section on the respective giant resonances. The maximum value of $3d_{3/2}$ is thus relatively larger than expected from the population ratio of the two $3d$ orbitals. After the shape resonance, the $3d_{3/2}$ photoionization cross section decreases continuously, apparently without showing any other maxima.

Our calculations included in Fig. 3 were shifted by −5.1 eV to facilitate comparison with the experiment, but have not been adjusted in any other way. As far as the sum of both components is concerned, the agreement between experiment and theory is very satisfactory, except for the region where the $3d_{3/2}$ channels begin to attain a measurable intensity. When comparing the spin-orbit-resolved cross-section calculations with the experiment, one has to remember that interchannel interactions have not been included in the former. This sheds a different light on the second local maximum in the $3d_{5/2}$ cross section. The impression that there is a local maximum seems to be caused by a preceding local minimum around 696 eV. In this energy region, the $3d_{5/2}$ curve lies clearly below, but the $3d_{3/2}$ curve slightly above, the calculated values. A possible explanation would then be that interchannel correlations between the two fine-structure components lead to a redistribution of intensity in this energy region. However, this explanation cannot account for all the discrepancy between experiment and theory. We also note that the steep onsets in the experimental partial photoionization cross sections seem to be underestimated in theory.

B. Auger electron yield

The determination of the photoionization cross section by measuring the Xe 3d and Ne 2p photoelectron spectra was rather slow; the measurements at each photon energy took about 2 h, and gave one or two points in Fig. 3. Unfortunately, it appeared that the determination suffered slightly from small changes in the photon energy during the lengthy scans. If the error bars above are also taken into account it proved not feasible to study the effect of the continuum excitations on the photoionization channels. The photoionization strengths were therefore also studied by an indirect, but much faster means, namely, by recording the yields of Auger electrons. Two measurements were made, one with the kinetic-energy window (width ~2.5 eV) centered at 521 and the other at 533 eV, which correspond to the M_5-$N_{4,5}N_{4,5}(^1D_2,^1G_4,^3P)$ and M_4-$N_{4,5}N_{4,5}(^1D_2,^1G_4,^3P)$ decay, respectively [31,32]. The results are shown in Fig. 4.

The Auger electron yields reproduce well the main features of the photoionization cross section curves (Fig. 3), including the second broad maximum at ~705 eV in the $3d_{5/2}$ cross section. All three sharp continuum resonances around 690 eV excitation energy are intense in the M_5 Auger yield. This indicates that they are predominantly connected with the ionization of the $3d_{5/2}$ shell. If the resonances were solely due to the $3d_{3/2}\rightarrow np, n\geqslant 6$ excitations, the following M_4-$N_{4,5}N_{4,5}$ resonant Auger decay processes would yield electrons whose kinetic energies are higher than those of the corresponding normal Auger processes, i.e., $E_{\mathrm{kin}}\geqslant 527$ eV [31,32]. (We can neglect the other two-hole one-particle final states, since the kinetic energies involved are either much too low or high.) The $3d_{3/2}\rightarrow np$ excitations may still play some role, as the first of the three resonances ($E_{\mathrm{exc}}\sim 686$ eV) also appears in the M_4 Auger yield. This yield also shows a hint of a continuum resonance at 698 eV, where there is a small shoulder in the absorption spectrum (Fig. 1). However, it must be noted that any other process resulting in electron emission at the same kinetic energies would also contribute to the yield spectra. Thus the peak at 678.5 eV in Fig. 4(b) originates from direct 4p photoionization and not from Auger decay.

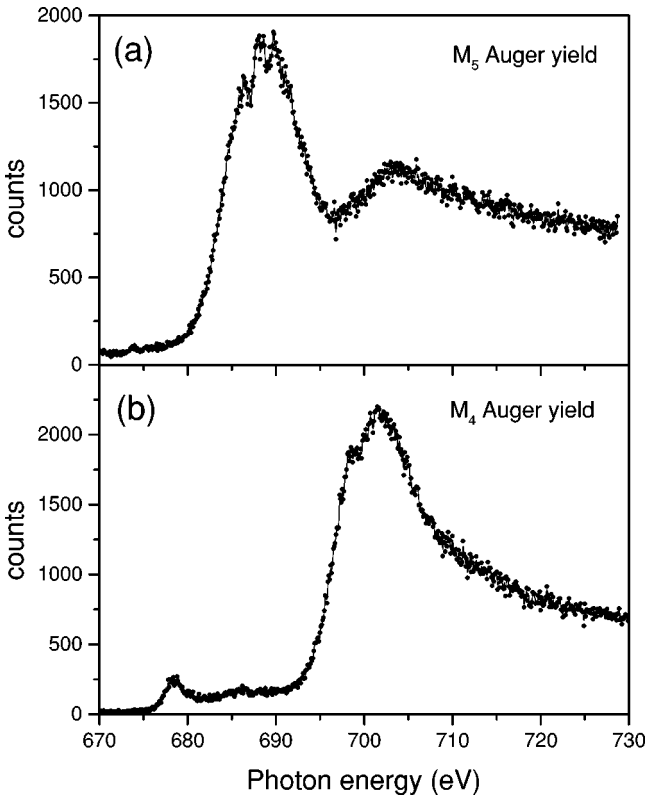

FIG. 4. Electron yield spectra of (a) 521-eV and (b) 533-eV electrons, corresponding to $M_5N_{4,5}N_{4,5}$ and $M_4N_{4,5}N_{4,5}$ Auger decay, respectively.

C. Angular distribution

The β values of the 3d photoelectron lines were calculated from Eq. (2) using $P=0.74$. The results are depicted in Fig. 5 as solid and open circles for $3d_{5/2}$ and $3d_{3/2}$, respectively. In addition, we show some previously unpublished results (open triangles) that were obtained with time-of-flight (TOF) spectroscopy at the HASYLAB, Hamburg. The TOF analyzers were positioned within the dipole plane. This geometry eliminates the effects of nondipole angular distribution parameters γ and δ.

The β values from the two different experiments are fairly similar. In the case of the X1B data, errors in the β measurements arise from irregularities of the relative yield of the anode sectors, inaccuracies in the determination of P, and statistical errors. Since the first factor diminishes by averaging over pairs of segments in Eq. (2), we estimate that the error in β values is at most ± 0.2 well above threshold. In the first few points of each β curve the error may be somewhat larger because of the low signal to background ratio. In the case of the HASYLAB data, imperfections of the normalization of the signal intensity in the different analyzers relative to each other lead to similar errors. The determinations of the β parameters using two different experimental setups clearly

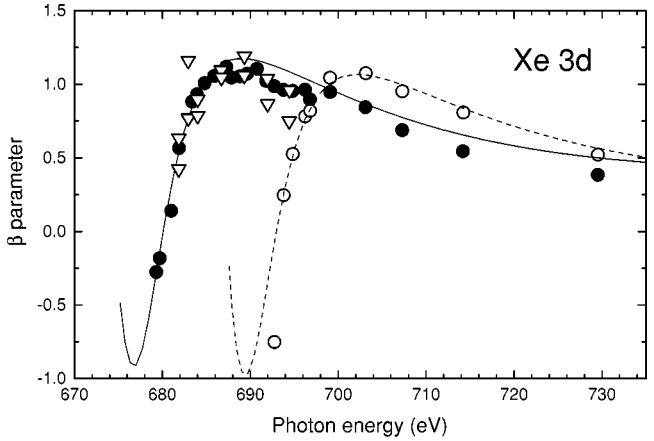

FIG. 5. The angular anisotropy parameters β of the $3d_{3/2,5/2}$ photoelectron lines. Closed and open circles give the experimental β values for the $3d_{5/2}$ and $3d_{3/2}$ photoelectron lines, respectively, determined from the measurements that were performed at the X1B beamline. Open triangles denote the two sets of β values for the $3d_{5/2}$ photoelectron line, extracted from the BW3 measurements. Solid and dashed lines depict the calculated β curves for $3d_{5/2}$ and $3d_{3/2}$ photoionization, respectively, shifted in energy by -2.0 eV.

agree within the error limits. As one of the instruments was operating in the dipole plane and the other was not, this confirms that nondipole effects in Xe $3d$ photoionization are not significant close to threshold, in accordance with theory [16].

Just like the partial cross sections, the angular anisotropy parameters β behave similarly for the two $3d$ photoelectron lines as a function of electron kinetic energy. Both of them obviously have negative values at very low kinetic energies, then rise rapidly until their maxima ($\beta \sim 1.1$) at 12–14 eV above threshold, after which they gradually decrease. This behavior is well reproduced by our single-channel calculations, except for the energy scale, which is shifted by -2.0 eV in Fig. 5. The calculations have been converted to a photon energy scale by using experimental values for the $3d$ ionization potentials; therefore, this shift, and the shift of -5.1 eV of the cross-section curve, are not easy to explain.

An oscillation of the dipole β parameter immediately at threshold was first predicted in Ref. [9]. The present calculation predicts that the anisotropy parameters of both $3d_{5/2}$ and $3d_{5/2}$ should have minimum values close to -1 within very few eV above the corresponding thresholds. It is not possible to confirm this experimentally due to very low $3d$ partial cross sections in this kinetic-energy region. However, as far as we could follow the β values toward threshold, they are in agreement with this prediction.

V. DISCUSSION AND CONCLUSIONS

High-resolution measurements of the Xe $3d_{5/2}$ and $3d_{3/2}$ partial cross section from below to 50 eV above threshold have clarified some questions arising from earlier work, and have revealed an interesting example of channel coupling within the same nonrelativistic configuration.

While our measurements reach a good agreement with the older measurements of Becker *et al.* [8] 50 eV above threshold, toward threshold we are able to reveal how both spin-orbit split components follow the two maxima in the photoabsorption cross section. Probably due to a much larger excitation bandpass, this could not be observed in the older data.

A number of theoretical photoionization studies of Xe $3d$ appeared during the last 30 years [9,28,33,34]. In the course of these studies, it became clear that the correct inclusion of relaxation effects is crucial for an adequate description of this process [28]. Coupling of $3d$ channels to other continuum channels seemed less important, which is again demonstrated by the good agreement of our own single-channel calculations with the experimental values. This can be rationalized by the large difference between the kinetic energies of the $3d$ photoelectrons and those resulting from the other channels, which in turn leads to large differences in the respective cross sections. Our experimental results for the sum of both Xe $3d$ components are in quantitative agreement with the relaxed relativistic random phase calculations of Kutzner *et al.* [28]; contrary to our model, the dip in the cross section around 695 eV also seems to be reproduced. This implies that interchannel interactions between both $3d$ components play a role around these photon energies, since the two calculations differ mainly by the inclusion of coupling between all Xe $5p$-$3d$ photoionization channels in Ref. [28]. This effect is in contrast to the spin-orbit branching ratio for most other noble gas subshells, which is influenced mainly by interaction with different nonrelativistic configurations.

The resonances preceding the $3d_{3/2}$ edge were interpreted as due to the $3d_{3/2} \rightarrow 6p,7p$ excitations [5,6]. However, this interpretation is not entirely satisfactory. First, the intensities of these excitations do not behave as expected for a Rydberg series, and are larger than those of the $3d_{5/2} \rightarrow 6p,7p$ excitations that are located below the $3d_{5/2}$ edge. Second, recent investigations on the $M_{4,5}$-$N_{4,5}N_{4,5}$ Auger electron spectra [7] revealed that the angular distribution of some normal Auger electron lines is affected by these resonances, implying a coupling with the direct $3d$ photoionization channel.

The present results also indicate that these resonances are connected with the single-hole $3d$ photoionization process. A possible explanation for the effect could be that the absorption features are due to double excitations involving the $4f$ orbital. The one-electron excitations $3d \rightarrow 4f$ cannot be observed in Xe, but they are very intense in barium due to the collapse of the $4f$ wave function [6,35]. Thus the behavior of the $4f$ wave function is sensitive to the charge state of the atom, and it could be the case that—also in two-hole two-electron configurations of Xe—the $4f$ wave function could collapse toward the nucleus so as to make double excitations rather likely. Tong, Li, and Pratt [36] predicted that the cross-section maximum of the $3d \rightarrow nf, \epsilon f$ excitations moves below ionization threshold in the Xe^+ ion, thus giving some credibility to the above suggestion. Recently, double excitations above the $4d$ threshold in xenon were also calculated to decay to the $4d^{-1}$ states [37]. Similar processes could then explain the preliminary observation that the $3d_{5/2}$ photoionization channel is affected by the resonances above

the corresponding ionization threshold. This tentative interpretation requires more theoretical and experimental support.

ACKNOWLEDGMENTS

A.K. would like to acknowledge the support from the Research Council for the Natural Sciences of the Academy of Finland. We are grateful to the Deutsche Forschungsgemeinschaft (DFG) for a postgraduate studentship (K.M.). The National Synchrotron Light Source at Brookhaven National Laboratory is supported by the U.S. Department of Energy, Division of Material Sciences and Division of Chemical Sciences.

[1] K. Siegbahn, C. Nordling, G. Johansson, J. Hedman, P. F. Hedén, K. Hamrin, U. Gelius, T. Bergmark, L. O. Werme, R. Manne, and Y. Baer, *ESCA Applied to Free Molecules* (North-Holland, Amsterdam, 1969).
[2] U. Gelius, J. Electron Spectrosc. Relat. Phenom. **5**, 985 (1974).
[3] S. Svensson, N. Mårtensson, E. Basilier, P. Å. Malmquist, U. Gelius, and K. Siegbahn, Phys. Scr. **14**, 141 (1976).
[4] R. D. Deslattes, Phys. Rev. Lett. **20**, 483 (1968).
[5] O. Yağci and J. E. Wilson, J. Phys. C **16**, 383 (1983).
[6] U. Arp, K. Iemura, G. Kutluk, T. Nagata, S. Yagi, and A. Yagishita, J. Phys. B **32**, 1295 (1999).
[7] J. Karvonen, A. Kivimäki, H. Aksela, S. Aksela, R. Camilloni, L. Avaldi, M. Coreno, M. de Simone, and K. C. Prince, Phys. Rev. A **59**, 315 (1999).
[8] U. Becker, H. G. Kerkhoff, M. Kupsch, B. Langer, D. Szostak, and R. Wehlitz, J. Phys. (Paris), Colloq. **48**, C9-497 (1987).
[9] D. J. Kennedy and S. T. Manson, Phys. Rev. A **5**, 227 (1972).
[10] K. J. Randall, J. Feldhaus, W. Erlebach, A. M. Bradshaw, W. Eberhardt, Z. Xu, Y. Ma, and P. D. Johnson, Rev. Sci. Instrum. **63**, 1367 (1992).
[11] C. T. Chen, Nucl. Instrum. Methods Phys. Res. A **256**, 595 (1987).
[12] J. Feldhaus, W. Erlebach, A. L. D. Kilcoyne, K. J. Randall, and M. Schmidbauer, Rev. Sci. Instrum. **63**, 1454 (1992).
[13] O. Hemmers, S. B. Whitfield, P. Glans, H. Wang, D. W. Lindle, R. Wehlitz, and I. A. Sellin, Rev. Sci. Instrum. **69**, 3809 (1998).
[14] K.-N. Huang, Phys. Rev. A **22**, 223 (1980).
[15] A. Bechler and R. H. Pratt, Phys. Rev. A **42**, 6400 (1990).
[16] J. W. Cooper, Phys. Rev. A **47**, 1841 (1993) [note that Eq. (24) of this paper contains errors].
[17] O. Hemmers, G. Fisher, D. L. Hansen, H. Wang, S. B. Whitfield, R. Wehlitz, J. C. Levin, I. A. Sellin, R. C. C. Perera, E. W. B. Dias, H. S. Chakraborty, P. C. Deshmukh, S. T. Manson, and D. W. Lindle, J. Phys. B **30**, L727 (1997).
[18] D. W. Lindle and O. Hemmers, J. Electron Spectrosc. Relat. Phenom. **100**, 297 (1999).
[19] F. Wuilleumier, Adv. X-Ray Anal. **16**, 63 (1973).
[20] O. Hemmers (private communication).
[21] G. B. Armen, J. Tulkki, T. Åberg, and B. Crasemann, Phys. Rev. A **36**, 5606 (1987).
[22] J. Jauhiainen, H. Aksela, S. Aksela, A. Kivimäki, O.-P. Sairanen, E. Nõmmiste, and J. Végh, J. Phys. B **28**, 3831 (1995).
[23] H. M. Köppe, A. L. D. Kilcoyne, J. Feldhaus, and A. M. Bradshaw, J. Electron Spectrosc. Relat. Phenom. **75**, 97 (1995).
[24] J. Tulkki, S. Aksela, H. Aksela, E. Shigemasa, A. Yagishita, and Y. Furusawa, Phys. Rev. A **45**, 4640 (1992).
[25] I. P. Grant, B. J. McKenzie, P. H. Norrington, D. F. Mayers, and N. C. Pyper, Comput. Phys. Commun. **21**, 207 (1980).
[26] B. K. Agarwal, *X-Ray Spectroscopy* (Springer-Verlag, Berlin, 1979).
[27] U. Becker, D. Szostak, H. G. Kerkhoff, M. Kupsch, B. Langer, R. Wehlitz, A. Yagishita, and T. Hayaishi, Phys. Rev. A **39**, 3902 (1989).
[28] M. Kutzner, V. Radojević, and H. P. Kelly, Phys. Rev. A **40**, 5052 (1989).
[29] B. Kempgens, B. S. Itchkawitz, W. Erlebach, H. M. Köppe, J. Feldhaus, and A. M. Bradshaw (unpublished).
[30] B. S. Itchkawitz, B. Kempgens, H. M. Köppe, J. Feldhaus, and A. M. Bradshaw, Rev. Sci. Instrum. **66**, 1531 (1995).
[31] L. O. Werme, T. Bergmark, and K. Siegbahn, Phys. Scr. **6**, 141 (1972).
[32] S. Aksela, H. Aksela, and T. D. Thomas, Phys. Rev. A **19**, 721 (1979).
[33] M. Ya. Amusia and V. K. Ivanov, Phys. Lett. **65A**, 217 (1978).
[34] A. Zangwill and D. A. Libermann, J. Phys. B **17**, L253 (1984).
[35] B. Sonntag, T. Nagata, Y. Sato, Y. Satow, A. Yagishita, and M. Yanagihara, J. Phys. B **17**, L55 (1984).
[36] X.-M. Tong, J.-M. Li, and R. H. Pratt, Phys. Rev. A **42**, 5348 (1990).
[37] H. Aksela, S. Alitalo, J. Jauhiainen, A. Kivimäki, T. Matila, T. Kylli, E. Nõmmiste, and S. Aksela, Phys. Rev. A **59**, R2563 (1999).